AEDC-TR-70-42

Copy 2

PROPAGATION OF ELASTO-PLASTIC STRESS WAVES IN CYLINDRICAL HIGH-PRESSURE SECTIONS

J. R. Baumgarten, J. R. DeWitt, and A. J. Cable

ARO, Inc.

August 1970

VON KÁRMÁN GAS DYNAMICS FACILITY
ARNOLD ENGINEERING DEVELOPMENT CENTER
AIR FORCE SYSTEMS COMMAND
ARNOLD AIR FORCE STATION, TENNESSEE

NOTICES

When U. S. Government drawings specifications, or other data are used for any purpose other than a definitely related Government procurement operation, the Government thereby incurs no responsibility nor any obligation whatsoever, and the fact that the Government may have formulated, furnished, or in any way supplied the said drawings, specifications, or other data, is not to be regarded by implication or otherwise, or in any manner licensing the holder or any other person or corporation, or conveying any rights or permission to manufacture, use, or sell any patented invention that may in any way be related thereto.

Qualified users may obtain copies of this report from the Defense Documentation Center.

References to named commercial products in this report are not to be considered in any sense as an endorsement of the product by the United States Air Force or the Government.

PROPAGATION OF ELASTO-PLASTIC STRESS WAVES IN CYLINDRICAL HIGH-PRESSURE SECTIONS

J. R. Baumgarten, J. R. DeWitt, and A. J. Cable
ARO, Inc.

FOREWORD

The research reported herein was sponsored by the Arnold Engineering Development Center (AEDC), Air Force Systems Command (AFSC), under Program Element 65401F, Project 876, Task G226.

The results presented were obtained by ARO, Inc. (a subsidiary of Sverdrup & Parcel and Associates, Inc.), contract operator of AEDC, Arnold Air Force Station, Tennessee, under Contract F40600-71-C-0002. The results of the research were obtained intermittently between June 1968 and July 1969, under ARO Project No. VT8002. The manuscript was submitted for publication on January 13, 1970.

This technical report has been reviewed and is approved.

Roy R. Croy, Jr.
Colonel, USAF
Director of Test

ABSTRACT

This report presents an analysis of the axisymmetric elastic and plastic stresses and deformations in thick wall cylindrical shells subjected to internal dynamic pressures. A direct numerical approach called the discontinuous-step analysis is used. This analysis is based on the direct use of the boundary conditions and the applicable physical laws to propagate dynamic changes in the cylinder by finite steps. Reflection of stress waves from both inner and outer boundaries is automatically generated. The validity of the method is checked by comparison of numerical results in the elastic range with published results for thick wall cylinders. Comparison is made with experimentally measured strains from the high-pressure section of a hypervelocity launcher. This analysis assumes that the work hardening of the material is independent of the strain rate and is constant for a large variation of plastic strain. Stress-strain relationships are derived for the condition of plane stress in the cylinder which is held to be representative of the actual conditions in the launcher high-pressure section. The digital computer program developed from this study predicts the distribution of dynamic stress and strain throughout the cylinder, the internal radial growth, the distribution of particle displacement, the distribution of yield stress in an autofrettaged cylinder, and the residual stress.

CONTENTS

APPENDIXES

I. ILLUSTRATIONS

Figure

Page

II. TABLES

NOMENCLATURE

A	Constant
A_i	Area, ith element sq in.
a_o	Inner radius, in.
b_o	Outer radius, in.
C_e	Elastic wave velocity, in./sec
C_j	Wave velocity elastic or plastic
C_p	Plastic wave velocity, in./sec
E_1	Elastic modulus, psi
E_2	Plastic modulus, psi
F	Force, lb
g	Gravitational constant, in./sec^2
K	Bulk modulus, psi
ℓ	Element length, in.
M	Mass, lb
P(t)	Transient internal pressure, psi
P	Internal pressure, psi
P_o	Step input pressure
r	Radius, in.
t	Time, sec
U_r^i	Radial growth ith element, in.
u	Particle displacement, in.
v	Particle velocity, in./sec
X_m	Total time interval of calculation, sec

Y	Original yield point, psi
δ	Arbitrary small constant, psi
ϵ	Strain, in./in.
ν	Poissons ratio
ρ	Density, lb/in.^{3}
σ	Stress, psi
σ_o	Work hardened yield point, psi
τ	Shear stress, psi

SUBSCRIPTS AND SUPERSCRIPTS

e	Elastic range
i	Index for identification of radial grid coordinate
m	Total number grid coordinates
p	Plastic range
r	Radial direction
x	Arbitrary radial direction
z	Longitudinal direction
θ	Tangential direction

SECTION I
INTRODUCTION

Mehta and Davids (Ref. 1) have investigated the propagation of transient stress waves in cylinders subjected to various types of dynamic loading. The study was limited to the elastic range of stress, and the authors employed their discontinuous-step analysis. A force balance and the stress-strain relations were formed as the basic governing phenomenon. These were used together with the proper boundary conditions to predict discrete changes in stress in finite time steps. With slight alteration, this is the method employed in the present study.

There are significant differences in the analysis of dynamic stress propagation for the plastic range as opposed to the elastic range. In the elastic state, the material retains constant properties of modulus, and the characteristic is well defined. In the plastic range, the modulus varies with the state of stress, and wave velocity changes from that of the elastic state. With the problem at hand, that of predicting the transient stress in the cylindrical high-pressure section of a hypervelocity launcher, both the elastic and plastic states of the material jointly exist in the higher pressure regimes. Any stress analysis must give cognizance to the fact that the cross section of the cylinder first becomes plastic at the core and, as pressure increases, the plastic boundary advances radially outward.

Davids, Mehta, and Johnson (Ref. 2) have investigated the propagation of transient stress waves in the elasto-plastic regime for a spherical body. In this case also, the authors applied their discontinuous-step analysis with emphasis on the solution of the radial displacement at the outside boundary of the sphere. An experiment was performed by the detonation of a charge placed within the cavity of a thick-wall aluminum sphere. Analytical and experimental results did not agree well, and the authors concluded that the analysis was only applicable for cases of loading of a nondecreasing nature (i. e., the rising portion of a pressure pulse). As will be indicated later, the present study removes this limitation from the discontinuous method.

SECTION II
BASIC EQUATIONS

2.1 ELASTIC RANGE

Consider a cross section of the cylindrical body as shown in Fig. 1a (Appendix I). The radial, tangential, and longitudinal stresses (σ_r, σ_θ, and σ_z) load an element as shown in Fig. 1b. In the problem at hand, the

internal impulsive pressure loading is caused by a piston moving along the longitudinal axis of the cylinder and compressing gas trapped therein. The principal loading is then radial in nature, and longitudinal strain is unimportant to the analysis. It is held that conditions of plane strain exist; hence, ϵ_z is zero. In the elastic range the stress-strain relations are then

$$\epsilon_\theta = \frac{1}{E_1} [\sigma_\theta - \nu(\sigma_z + \sigma_r)] \tag{1}$$

$$\epsilon_r = \frac{1}{E_1} [\sigma_r - \nu(\sigma_\theta + \sigma_z)] \tag{2}$$

$$\epsilon_z = 0 = \frac{1}{E_1} [\sigma_z - \nu(\sigma_\theta + \sigma_r)] \tag{3}$$

Substituting for σ_z from Eq. (3) yields

$$\sigma_r = \frac{E_1}{(1+\nu)(1-2\nu)} [(1-\nu)\epsilon_r + \nu\epsilon_\theta] \tag{4}$$

and

$$\sigma_\theta = \frac{E_1 (1-\nu)}{(1+\nu)(1-2\nu)} \left[\epsilon_\theta + \epsilon_r \frac{\nu}{1-\nu}\right] \tag{5}$$

Equations (4) and (5) relate the radial and tangential stress to the strains.

2.2 PLASTIC RANGE

Following Hopkins (Ref. 3, page 128), a work hardening model is assumed for the stress-strain relation of the material. Let the stress-strain curve of the steel in uni-axial loading be as shown in Fig. 2. Here the effects of rate of strain and rate of hardening are neglected. The plastic modulus E_2 is taken as constant in this assumption of linear strain hardening.

The plastic strains for the small cylindrical segment are taken to be incompressible (see Hopkins, Ref. 3, page 113). Then, for plain strain,

$$\epsilon_r^p + \epsilon_\theta^p = 0 \tag{6}$$

but the total strain is the sum of the plastic and elastic strain,

$$\epsilon_r = \epsilon_r^p + \epsilon_r^e \text{ and } \epsilon_\theta = \epsilon_\theta^p + \epsilon_\theta^e \tag{7}$$

Combining Eqs. (6) and (7), we have

$$\epsilon_r - \epsilon_\theta = \epsilon_r^e + \epsilon_\theta^e \tag{8}$$

Now, from Eqs. (1) and (2) for the plane strain case

$$\epsilon_r^e = \frac{1+\nu}{E_1}[\sigma_r(1-\nu) - \nu\sigma_\theta] \tag{9}$$

$$\epsilon_\theta^e = \frac{1+\nu}{E_1}[\sigma_\theta(1-\nu) - \nu\sigma_r] \tag{10}$$

Substituting Eqs. (9) and (10) into (8), one finds the bulk compressibility relation for the cylindrical plain strain case as

$$\sigma_r + \sigma_\theta = \left(\frac{3K}{1+\nu}\right)(\epsilon_r + \epsilon_\theta) \tag{11}$$

Now for the elastic state, one may assume a simple Tresca yield criterion (point A, Fig. 2). The principal strain, depicted in Fig. 3a, exists in the r-θ plane and the yield criterion is

$$\sigma_\theta - \sigma_r = Y \tag{12}$$

Realizing that this criterion attains only in the elastic range or for a perfectly plastic material, one sets to the task of modifying the criterion to relate stress and strain in the plastic range (point C, Fig. 2). The yield criterion is of the form

$$\sigma = Y' + E_2(\epsilon) \tag{12a}$$

where σ is the principal stress and ϵ is the equivalent total strain (Ref. 4). Under these assumptions, Eq. (12a) becomes

$$\sigma_\theta - \sigma_r = \left(1 - \frac{E_2}{E_1}\right)Y + \left(\frac{\epsilon_\theta - \epsilon_r}{1+\nu}\right)E_2 \tag{12b}$$

Combining Eqs. (11) and (12b), one obtains expressions for stress in terms of total strain in the plastic state. Thus,

$$\sigma_r = \frac{(3K - E_2)}{2(1+\nu)}\epsilon_\theta + \frac{(3K + E_2)}{2(1+\nu)}\epsilon_r - \left(1 - \frac{E_2}{E_1}\right)Y/2 \tag{13}$$

and

$$\sigma_\theta = \frac{(3K + E_2)}{2(1+\nu)}\epsilon_\theta + \frac{(3K - E_2)}{2(1+\nu)}\epsilon_r + \left(1 - \frac{E_2}{E_1}\right)Y/2 \tag{14}$$

2.3 MOMENTUM BALANCE

The essence of the discontinuous-step method consists of defining the force difference on a given element from the known instantaneous stress distribution. In a given time increment, this force creates an impulse (force x time) giving rise to a change in momentum of the element (mass x change in velocity). Considering the semicylindrical element of Fig. 3, the net force acting in a given direction is (Ref. 1)

$$F_x = [(\sigma_r^{i+1}(2r_{i+1}\ell) - \sigma_r^i(2r_i\ell) - \sigma_\theta^i(2r_{i+1} - 2r_i)\ell]$$

Now, the inner surface area of the ith element is given by

$$A_i = \pi r_i \ell$$

and the net force may be written

$$F_x = \frac{2}{\pi}[(\sigma_r^{i+1}A_{i+1} - \sigma_r^i A_i) - \sigma_\theta^i(A_{i-1} - A_i)]$$

Now, the impulse-momentum relations equate the total impulse $F_x dt$ to the momentum $m_i d\bar{v}$ of the mass center. The mass center of the semicylindrical element of radius R is located on the x axis (Fig. 3) at $\bar{R} = 2R/\pi$. Then

$$M_i d\bar{v} = F_x dt$$

and

$$\frac{d\bar{v}}{dt} = \frac{2}{\pi}\frac{dv}{dt}$$

Substituting in the expression for F_x and canceling $2/\pi$, we have

$$dv = [(\sigma_r^{i+1}A_{i+1} - \sigma_r^i A_i) + \sigma_\theta^i(A_i - A_{i+1})]dt/M_i \qquad (15)$$

where M_i, the mass of the ith element is

$$M_i = \frac{\rho\pi}{2}\left[r_{i+1}^2 - r_i^2\right]\ell$$

By use of Eq. (15), one can define the incremental change in particle velocity dv that occurs in a given time increment as the result of the radial and tangential stress distribution.

2.4 STRESS PROPAGATION

As indicated in Fig. 3, one first divides the cylinder into a finite number of elements i_m. This radial grid is then fixed in time, and the cells within the grid assume instantaneous states of strain in the elastic or plastic region depending on the internal pressure and the elapsed time. The state of any cell can be defined at any time by assigning the variables of particle displacement u, particle velocity v, strain ϵ, and stress σ. Additionally, the state of any cell, of width dr, can be changed over a time increment dt by defining the incremental change in displacement du, velocity dv, and strain $d\epsilon$.

In the radial coordinate set used, the tangential and radial strains are by definition (Ref. 5),

$$\epsilon_\theta = \frac{u}{r} \text{ and } \epsilon_r = \frac{du}{dr}$$

In starting the iteration process, an impulse of pressure P(t) is given to the core of the cylinder in the first time increment. This gives rise to a stress wave having the elastic wave velocity

$$C_e = \left(\frac{E}{\rho} \frac{(1-\nu)}{(1+\nu)(1-2\nu)} \right)^{1/2} \tag{16}$$

or the plastic wave velocity (Ref. 3, Eq. 6.40)

$$C_p = \left(\frac{K(1 + E_2/3K)}{(1 - E_2/9K)\rho} \right)^{1/2} \tag{17}$$

depending on the magnitude of the principal stress.

In a given time t, the state of the system is examined at each individual cell. If the radial velocities of two adjacent cells i and i + 1 are v_i and v_{i+1}, respectively, from the basic definition of radial strain one can define an average radial strain increment $d\epsilon_r$ during the time interval dt by

$$d\epsilon_r = (v_{i+1} - v_i) \frac{dt}{dr}, \quad i = 1, 2, \ldots i_m \tag{18}$$

where dr is the constant radial grid increment. Since the element may already be strained at the beginning of the time interval dt by an amount ϵ_r^{i+1}, the new strain level at the end of the increment $\left(\epsilon_r^{i+1}\right)'$ at the end of the interval is the cumulation

$$(\epsilon_r{}^{i+1})' = \epsilon_r{}^{i+1} + d\epsilon_r$$

Then, the state of strain at the end of the time interval is reinitiated by replacing the old level by the new level, or using the replacement symbol,

$$\epsilon_r^{i+1} \leftarrow \epsilon_r^{i+1} + d\epsilon_r \tag{19}$$

Similarly, from the mathematical definition of tangential strain,

$$d\epsilon_\theta = v_i \frac{dt}{r_i} \tag{20}$$

and the corresponding cumulation condition is

$$\epsilon_\theta^i \leftarrow \epsilon_\theta^i + d\epsilon_\theta \tag{21}$$

Finally, the incremental change of velocity dv occurring over a time interval is defined from Eq. (15), and velocity is cumulatively updated with

$$v_i \leftarrow v_i + dv \tag{22}$$

Relations (19), (21), and (22) form the essential basis for the discontinuous-step analysis. One needs only to direct these operations repetitively for $i = 1$ to $i = i_m$ in a given time interval, then update the time

$$t \leftarrow t + dt$$

continuing over the time span of interest. Additional statements are necessary to adjust the strain increments when the plastic range is reached and to control the selection of the constant radial mesh width dr. One must also be aware of the sequential ordering of operations which is of critical importance. These final contingencies will now be discussed.

SECTION III
NUMERICAL PROCEDURE

The first choice facing the analyst is in the selection of the grid mesh width dr and the time increment dt. Contrary to the practice adopted by Mehta and Davids (Refs. 1 and 2) the present study fixes the time increment dt and the mesh width dr from the outset and retains these two dimensions as fixed regardless of the state of stress, either plastic or elastic. The usual characteristic assumption is

$$dr = C_j dt$$

where C_j is the appropriate wave velocity for the elastic or plastic state. It should be noted that plastic wave velocity is less than elastic. For a fixed time interval, the radial increment dr would change (drop) when the material became plastic, leading to confusion in previously accumulated stress based on the original grid mesh.

Previous investigations (Refs. 6 and 7) concerned with wave phenomena involving hyperbolic equations have shown that computations are stable if

$$dr \geq C_j dt$$

From this fact, an appropriate time increment is chosen, and a radial increment dr is set such that it is greater than the elastic wave (fastest) advance in this preselected time interval. For computational purposes, we have

$$dr = A\, C_e dt$$

where A is a constant greater than unity, such that $dr > (dr)_e > (dr)_p$.

The computer program, written for this study, has the following sequence of operations:

(1) Specify given data: a_o, b_o, ℓ, ρ, E_1, E_2, ν, dt,

(2) Specify radial distribution of yield point, σ_o and initial values of σ_r and σ_θ, ϵ_r and ϵ_θ, if auto-frettaging exists.

(3) Define

$$dr = A\, C_e dt$$

$$m = \frac{b_o - a_o}{dr}$$

$$r_{i+1} = r_i + dr$$

$$A_i = \pi r_i \ell$$

$$M_i = \frac{1}{2}\rho\pi\left[r_{i+1}^2 - r_i^2\right]\ell$$

(4) Define pulse input P = P(t)
then $\sigma_r^1 = -P$ (boundary condition)

(5) Propagation procedure: repeat steps A through L for $i = 1$ to $i = i_m$.

A. Increment radial strain $d\epsilon_r = \dfrac{(v_{i+1} - v_i)dt}{dr}$

B. Accumulate radial strain

$$\epsilon_r^{i+1} \rightarrow \epsilon_r^{i+1} + d\epsilon_r$$

C. Define radial and tangential stresses

(1) Elastic State

$$\sigma_r^{i+1} = \frac{E_1}{(1-\nu-2\nu^2)}[\epsilon_r^{i+1}(1-\nu) + \nu\epsilon_\theta^i]$$

$$\sigma_\theta^i = \frac{E_1}{(1-\nu-2\nu^2)}[\nu\epsilon_r^{i+1} + (1-\nu)\epsilon_\theta^i]$$

(2) Plastic State

$$\sigma_r^{i+1} = \frac{(3K-E_2)}{2(1+\nu)}\epsilon_\theta^i + \frac{(3K+E_2)}{2(1+\nu)}\epsilon_r^{i+1} - \left(1 - \frac{E_2}{E_1}\right)Y/2$$

$$\sigma_\theta^i = \frac{(3K+E_2)}{2(1+\nu)}\epsilon_\theta^i + \frac{(3K-E_2)}{2(1+\nu)}\epsilon_r^{i+1} + \left(1 - \frac{E_2}{E_1}\right)Y/2$$

D. Apply boundary corrections[1]: for i = 1 and i = i_m only

(1) Elastic State

$$\sigma_\theta^i = \frac{1}{1-\nu^2}[E_1\epsilon_\theta^i + \nu(1+\nu)\sigma_r^i]$$

(2) Plastic State[2]

$$\sigma_\theta^i = \sigma_o\left(1 - \frac{E_2}{E_1}\right) + \epsilon_\theta^i\left(\frac{E_2}{1+\nu}\right)$$

---

[1]Required because of boundary condition 4 and defined from Hooke's Law, Eq. (1).

[2]Defined from bulk compressibility relation and plastic yield criterion, Eqs. (11) and (12b).

E. Apply boundary correction: for $i = i_m$ only

$$\sigma_r^{i+1} = 0$$

F. Define tangential strain increment

$$d\epsilon_\theta = \frac{v_i dt}{r_i}$$

G. Cumulate tangential strain

$$\epsilon_\theta^i \leftarrow \epsilon_\theta^i + d\epsilon_\theta$$

H. Define velocity increment

$$dv = [(\sigma_r^{i+1} A_{i+1} - \sigma_r^i A_i) + \sigma_\theta^i (A_i - A_{i+1})] \frac{dt}{M_i}$$

I. Cumulate particle velocity

$$v_i \leftarrow v_i + dv$$

J. Define radial displacement increment

$$du_r = v_i dt$$

K. Cumulate radial displacement

$$u_r^i \leftarrow u_r^i + du_r$$

L. Increment Time

$$t \leftarrow t + dt$$

Steps A through L are repeated for a specified time interval to $t = X_m$. If the induced longitudinal stress is desired for this plane strain case, it can be found from

$$\sigma_z^i = \nu(\sigma_r^{i+1} + \sigma_\theta^i)$$

A particular procedure is followed when stress levels reach the plastic state as defined by the usual Tresca yield criterion (see Ref. 2, page 131). Referring to Fig. 2, the state of stress represented by point B is not possible physically. When a new strain increment $d\epsilon_r$ at some time interval indicates that the plastic condition attains, stress is now calculated by step 5C(2) and the stress-strain relationship is established by the line AC.

At this point in the analysis, judgment is made on the amount of work hardening which has attained. The total principal stress is investigated, and the yield point Y is updated to a new yield point σ_o defined by

$$\sigma_o^i = (\sigma_\theta^i - \sigma_r^{i+1})$$

Thus, a radial array of work hardening is one of the results of a given computer run. As strain is relieved with decreasing internal pressure, elastic relief is allowed from point C, Fig. 2. Additionally, it is possible to prestore a radial distribution of work hardened yield points σ_o^i and residual stresses and strains at the outset of computations. This is representative of an autofrettaged cylinder (step 2). The final distribution of residual stress and strain, work hardened yield points and displacements can be retained for subsequent transient pressure loadings of the cylindrical section if required.

SECTION IV
RESULTS AND DISCUSSION

In order to check the accuracy of the derivations and the program, comparison was made with published solutions for thick wall cylinders. The literature only contains solutions limited to the elastic range; hence, this part of the analysis could be verified.

Figure 4 gives the solution for dimensionless tangential stress at the inner radius a_o for a cylinder of outer radius $b_o = 2a_o$. The core is given a step input of pressure at time zero. The solution from this study, using the discontinuous-step analysis, is compared with that of Chou and Greif (Ref. 7) obtained from a method of characteristics. The interested reader should refer to Fig. 4, page 1071 of Ref. 7 in which the authors compare the results of Mehta and Davids (Ref. 1) with their solution. The present study, using the same discontinuous-step analysis, shows much improved results over those of Mehta and Davids (Ref. 1) shown in Fig. 4 of Ref. 7. Correction of an error in Eq. 16e of Ref. 1 and revised rules on selection of mesh width dr are held to account for the improvement.

In order to load the cylinder internally, it is necessary to know the transient gas pressure in the high-pressure section of the launcher. Pressures here are so severe as to preclude measurement with conventional transducers. Failing to know the pressure-time signature from experiment for any given launch cycle, one uses predicted pressures. These predicted pressures are obtained from a real gas analysis of the cycle after DeWitt and Cable (Ref. 8). Figures 5 and 6 show plots of pressure from analysis which corresponds best to measured piston velocity and launch velocity for two shots of a hypervelocity launcher at AEDC. Each transient pressure load was approximated by a series of straight lines shown in the figures. This allowed the determination of instantaneous pressure as a function of time from a subroutine algorithm.

Figures 7 and 8 compare the measured tangential strain, ϵ_θ, at the periphery of the high-pressure section of the launcher with the calculated strain. The strain gages were located in the region of highest loading. The transient internal pressures were taken from Figs. 5 and 6, respectively. Comparison shows that predicted peak strain agrees well with peak measured strain. The time duration of the pressure pulse in the analysis corresponds with that of the measured transient strain. In each case, the computed results for the autofrettaged cylinder are in better agreement with measured results. The reader should consider that measurements were made on a fully autofrettaged section.

Figures 7 and 8 show a high frequency ripple superimposed on the general transient response. Investigation shows that this frequency corresponds very well with the fundamental ring or hoop frequency for the dimensions of the cylinder. Its period is significantly that time required for a transient pulse to be transmitted to the outer boundary and reflected to the core.

A study was made of the effects of autofrettaging on the thick-walled radial section. Figure 9 compares the computed residual stress remaining in the hypothetical study of two launch cycles of increasing severity. The subtlety here is that the lower pressure cycle (194×10^3 psi) is first applied to a virgin section. Wall yielding occurs, the transient pressure disturbance subsides, and the new equilibrium state of static radial and tangential residual stress (solid lines) is predicted from the basic force balance. This radial stress distribution is prestored prior to the subsequent computer analysis of a higher pressure launch cycle (221×10^3 psi). Figure 9 shows the new computed residual stress remaining after the second launch cycle. As expected, the cylinder is further autofrettaged and peak radial and tangential residual stress are increased. The first launch cycle yielded the wall through 42 percent of its thickness.

The second shot increased the plastic radius to 52 percent of the wall thickness. This corresponds well with the location of the abrupt slope change in the σ_θ curves of Fig. 9.

Table I (Appendix II) lists the predicted bore growth of the cylinder from the analytical pressure pulses of shots T-1237 and T-1247 (Figs. 5 and 6, respectively). The table compares the growth for a virgin section and for an autofrettaged section. In each case, the autofrettaged section showed less radial growth. Table II compares the peak external tangential strains for each of the shots listed. It is seen that previous strain history directly affects the dynamic response. The autofrettaged section showed significantly less peak strain. It is held that the large radial region, having higher yield points from work hardening, remains elastic for higher pressure excursions. Hence, the autofrettaged section sees less strain induced for the same internal pressure distribution. The experimental measurements are in good agreement with the prediction for the autofrettaged section.

SECTION V
RECOMMENDATIONS

In order to provide for the effects of strain rate on the stress-strain characteristics of the steel, the present mathematical model should be expanded. A Voigt model, or perhaps a combinational Zener model, could be considered in the momentum balance of the radial element. Thus

$$M\,d\bar{v} = F\,dt - \eta\dot{\epsilon}\,dt$$

where η is the appropriate loss coefficient for the material.

REFERENCES

1. Mehta, P. K. and Davids, N. "A Direct Numerical Analysis Method for Cylindrical and Spherical Elastic Waves." AIAA Journal, Vol. 4, No. 1, January 1966, pp. 112-117.

2. Davids, N., Mehta, P. K., and Johnson, O. T. "Spherical Elasto-Plastic Waves in Materials." Proceedings of Colloquium, Behavior of Materials Under Dynamic Loading, November 9, 1965, ASME, pp. 125-137.

3. Hopkins, H. G. Progress in Solid Mechanics. Vol. 1, I. N. Sneddon and R. Hill, Eds., North-Holland Publishing Company, Amsterdam, 1960, Chapter III.

4. Mendelson, A. and Manson, S. S. "Practical Solutions of Plastic Deformation Problems in Elastic-Plastic Range." NACA TN 4088, September 1957.

5. Timoshenko, S. Theory of Elasticity. McGraw-Hill Book Company, 1934, Chapter 3, Section 26, p. 62.

6. Von Neuman, J. and Richtmeyer, R. D. "A Method for the Numerical Calculation of Hydrodynamic Shocks." Journal of Applied Physics, Vol. 1, 1950, p. 232.

7. Chou, S. C. and Greif, R. "Numerical Solution of Stress Waves in Layered Media." AIAA Journal, Vol. 6, No. 6, June 1968, pp. 1067-1074.

8. DeWitt, J. R. and Cable, A. J. "A Comparison of Experimental and Theoretical Launcher Kinematics." AEDC-TR-65-203 (AD470966), Arnold Air Force Station, Tennessee.

APPENDIXES

I. ILLUSTRATIONS
II. TABLES

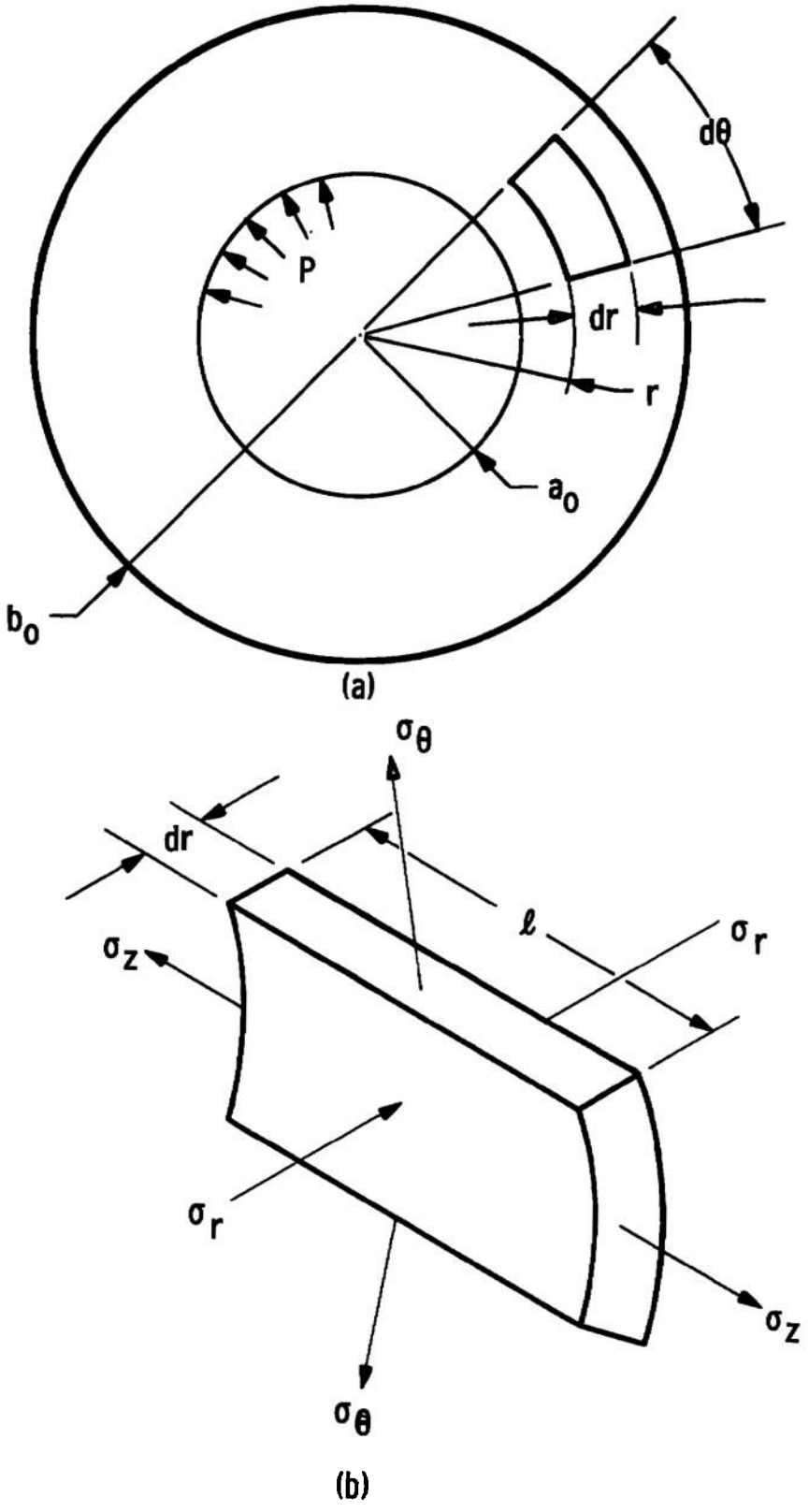

Fig. 1 Nomenclature of Cylindrical Cross Sections

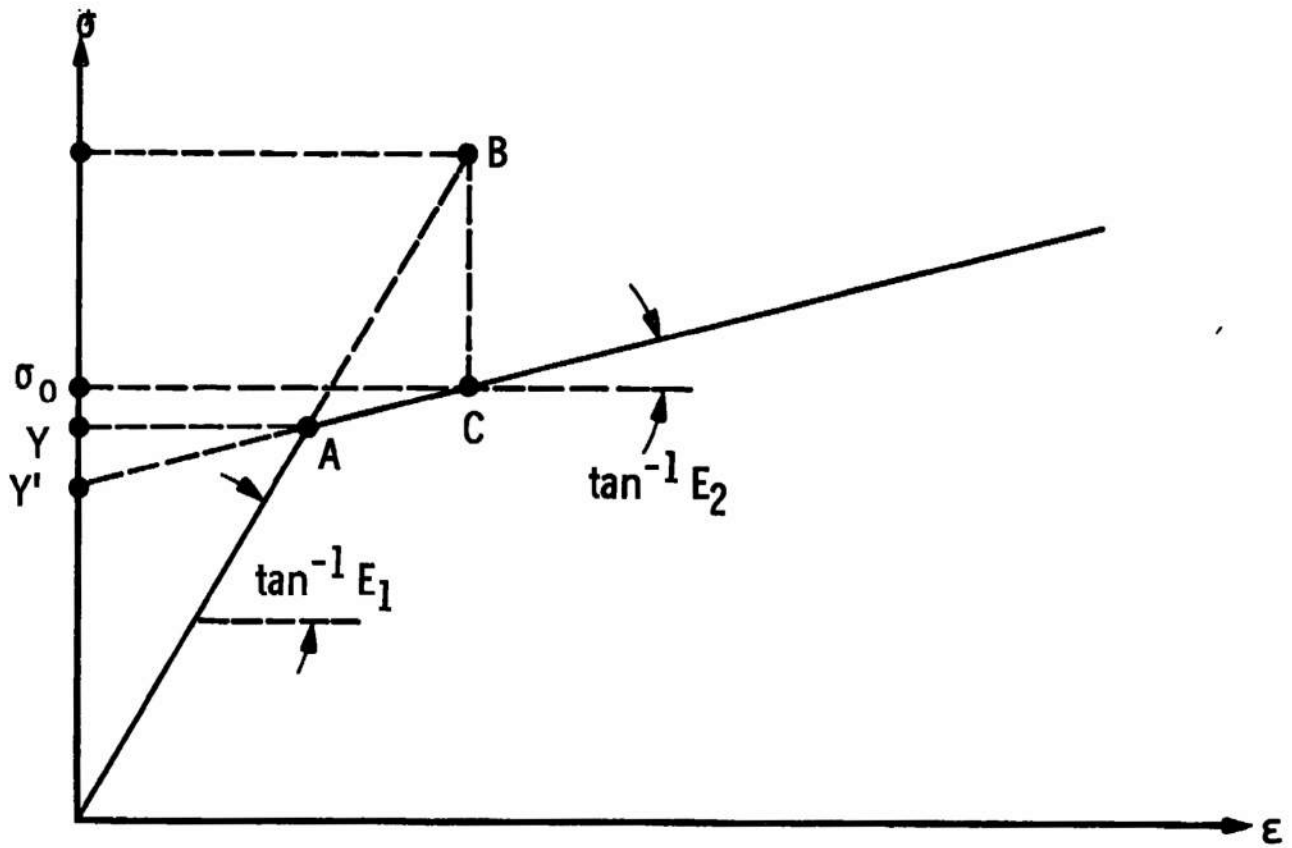

Fig. 2 Stress-Strain Curve for Ductile Steel

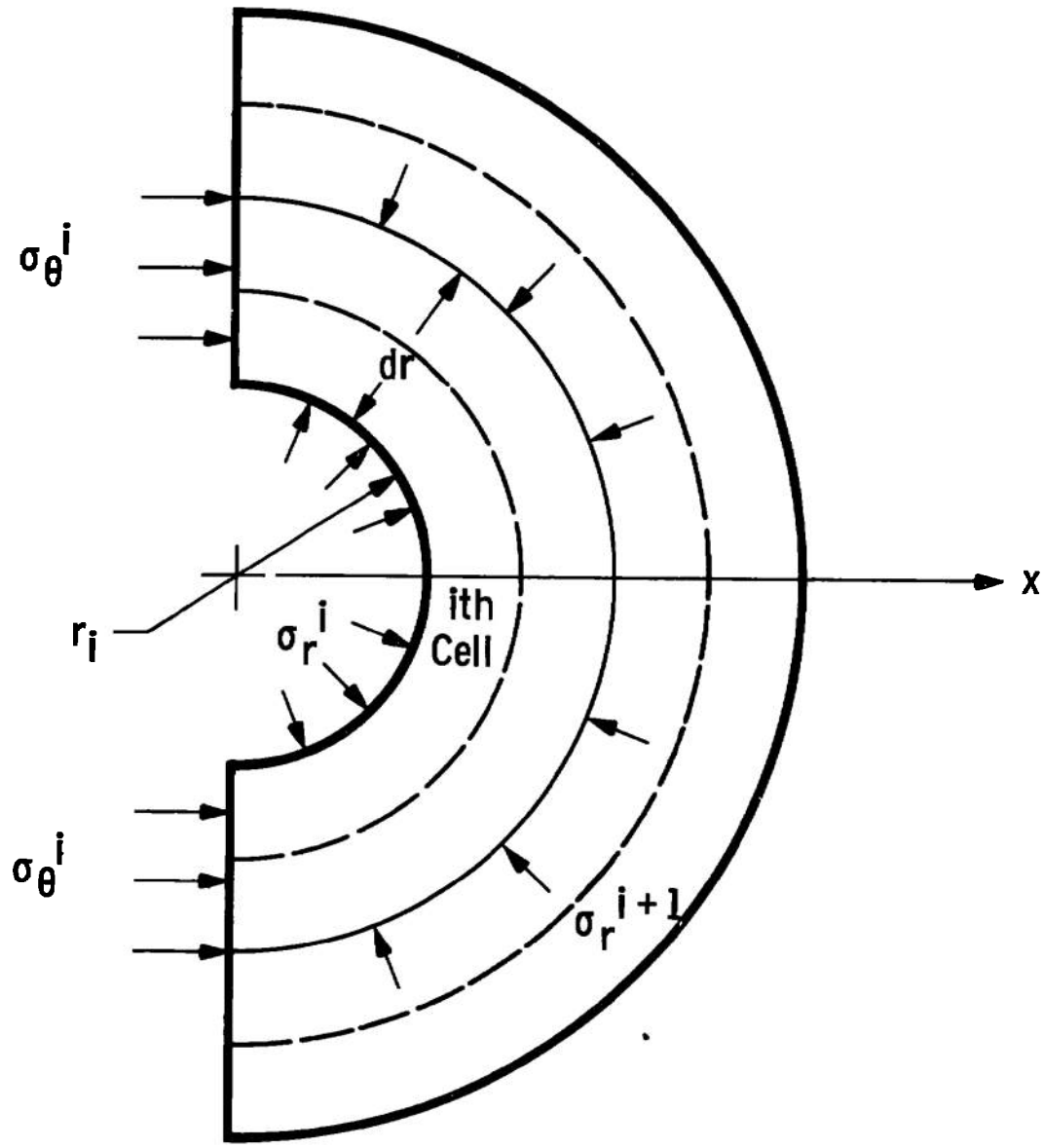

Fig. 3 Force Balance on Semicircular Element

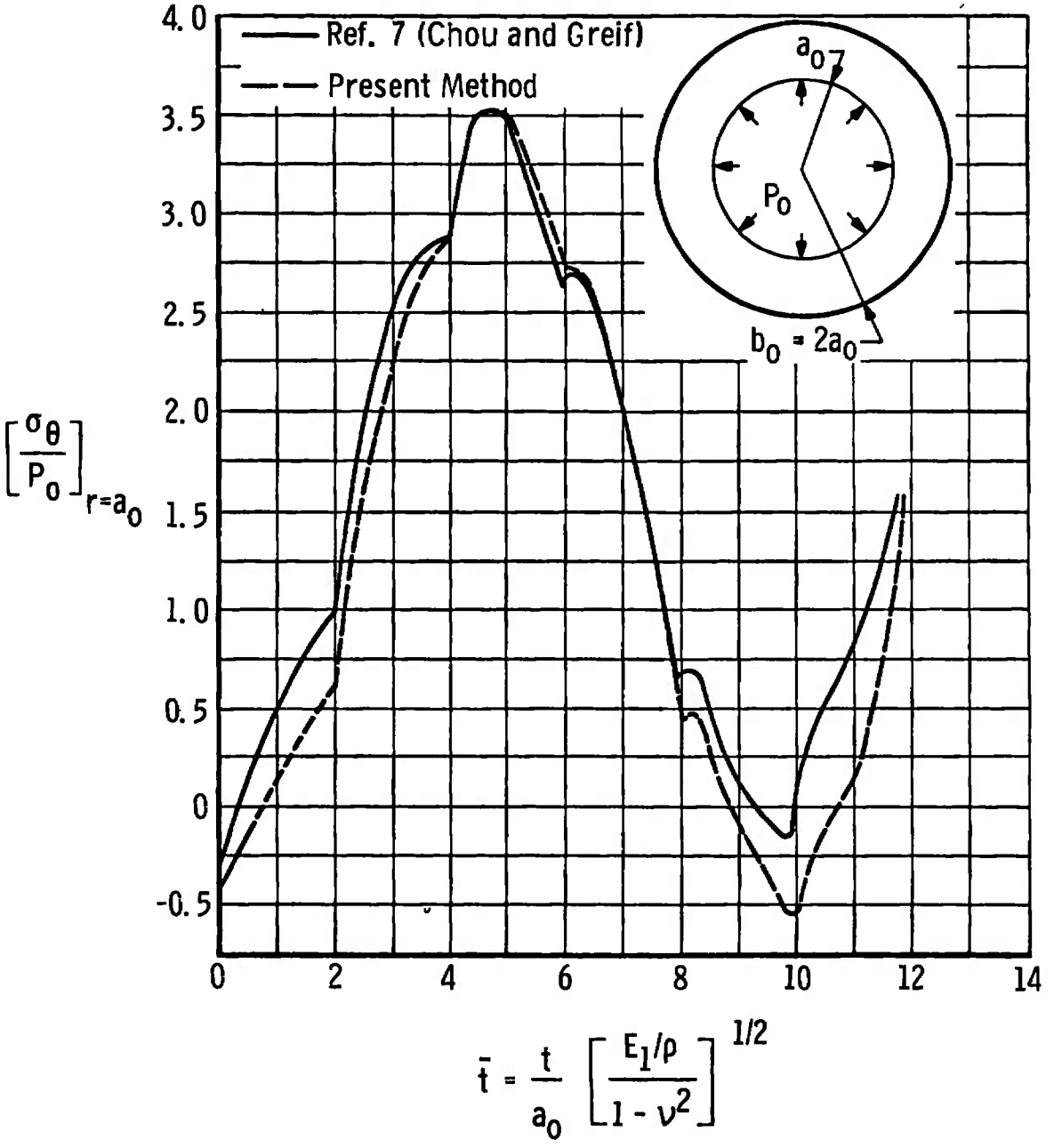

Fig. 4 Response of Cylinder to Step Input P_o. Comparison of Solution by Characteristics (Chou and Grief) and Discontinuous Step Method

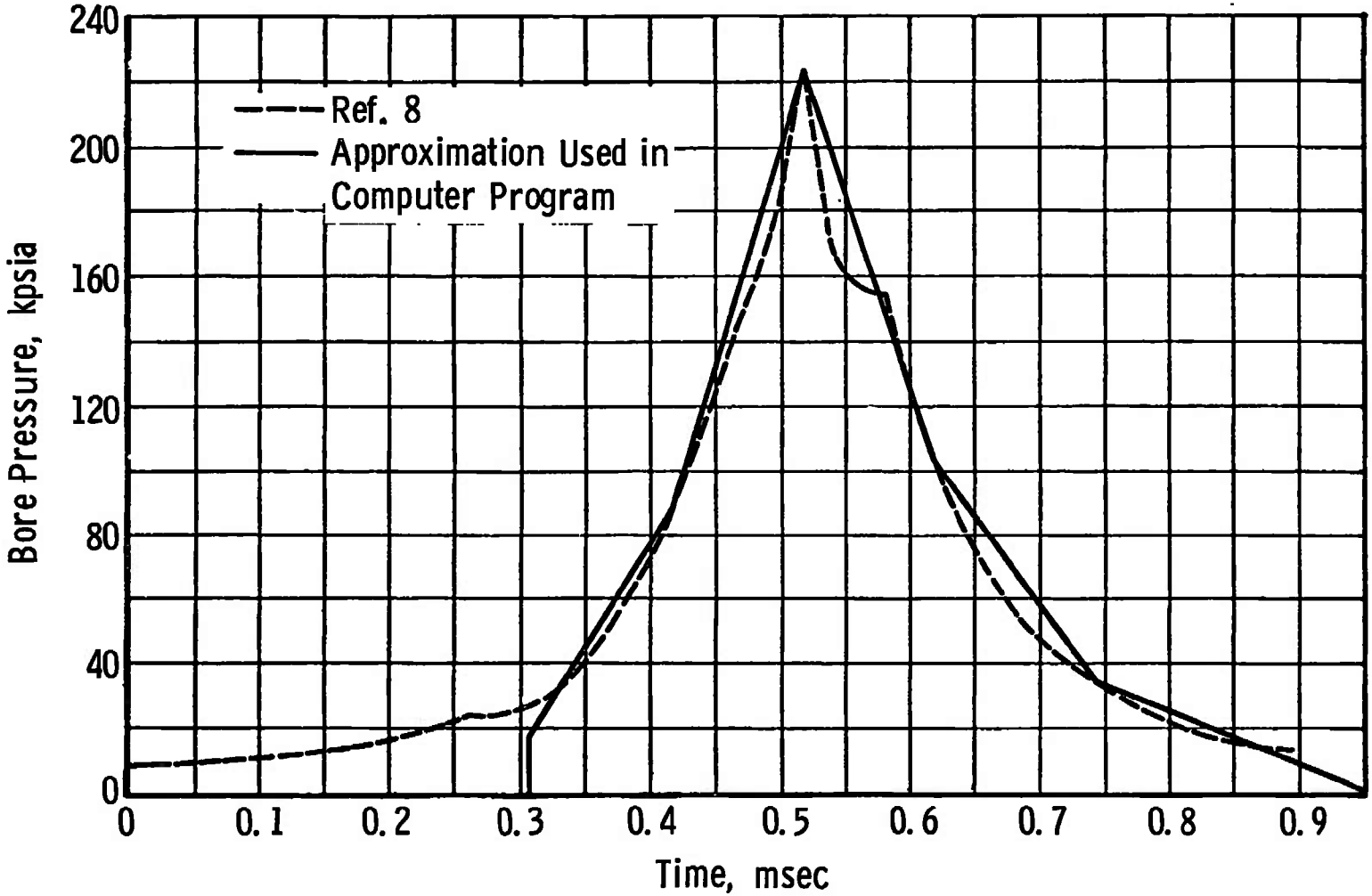

Fig. 5 Pressure versus Time Distribution Approximating to Shot T 1237 (221,000-psia Peak Pressure)

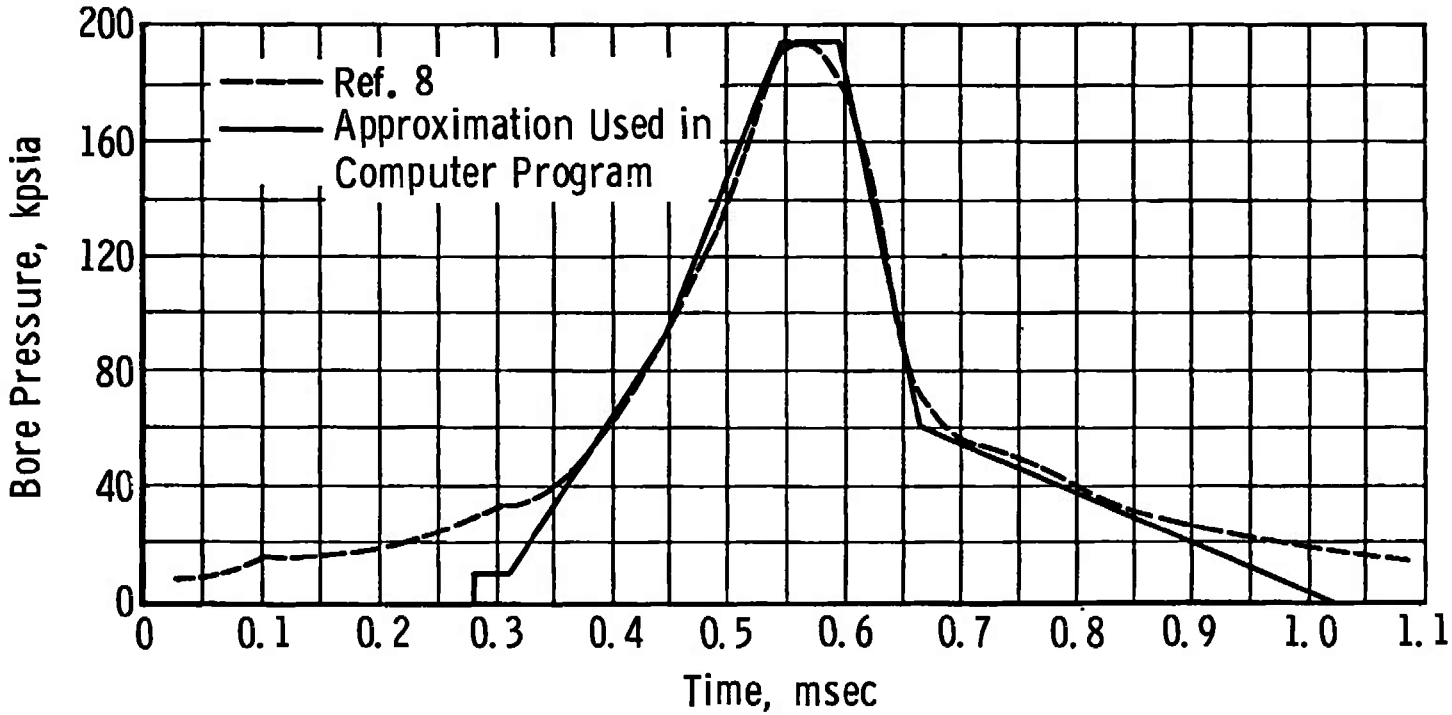

Fig. 6 Pressure versus Time Distribution Approximating to Shot T 1247 (194,000-psia Peak Pressure)

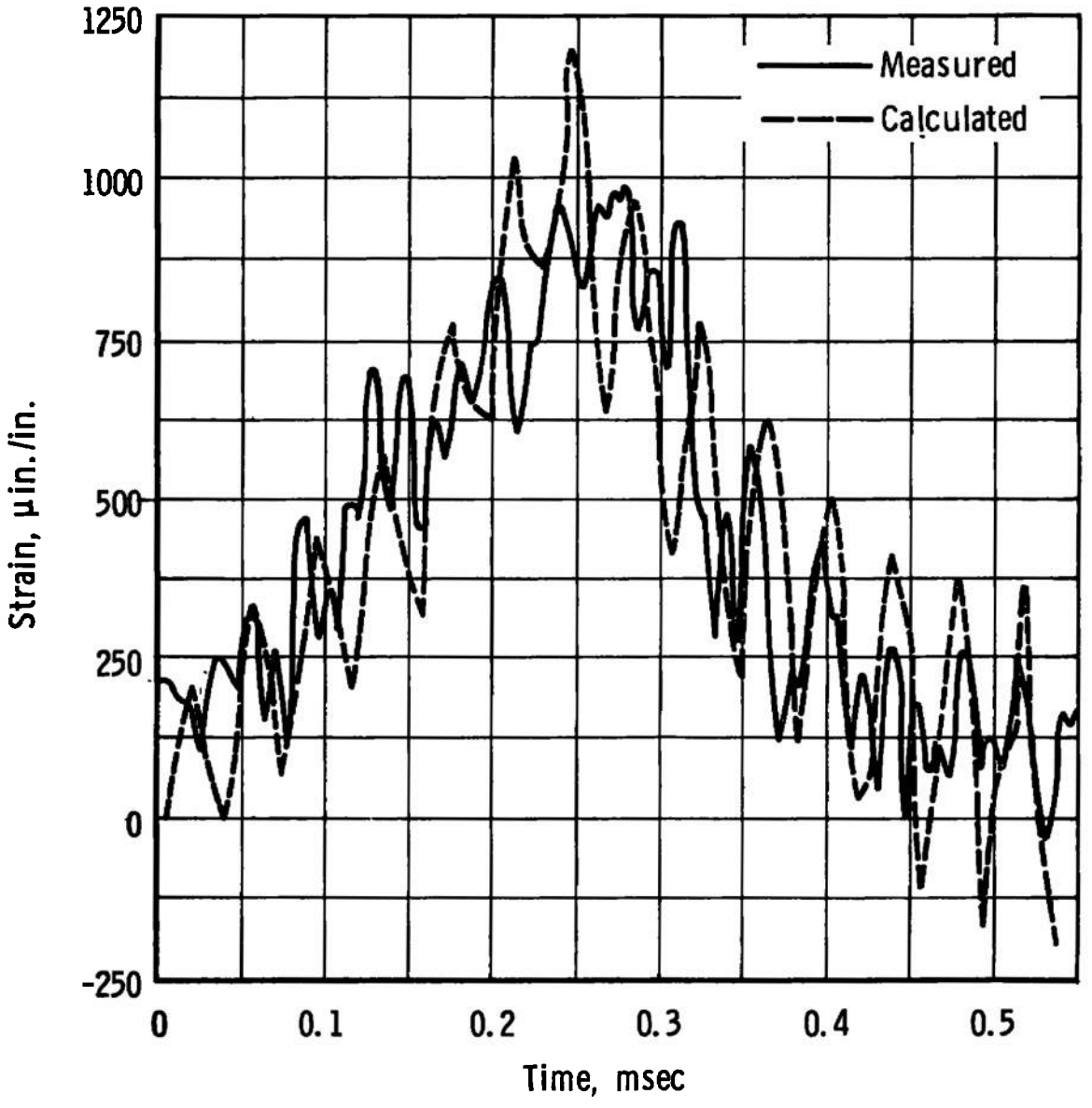

Fig. 7 Comparison of Measured and Calculated Strain for Shot T-1237

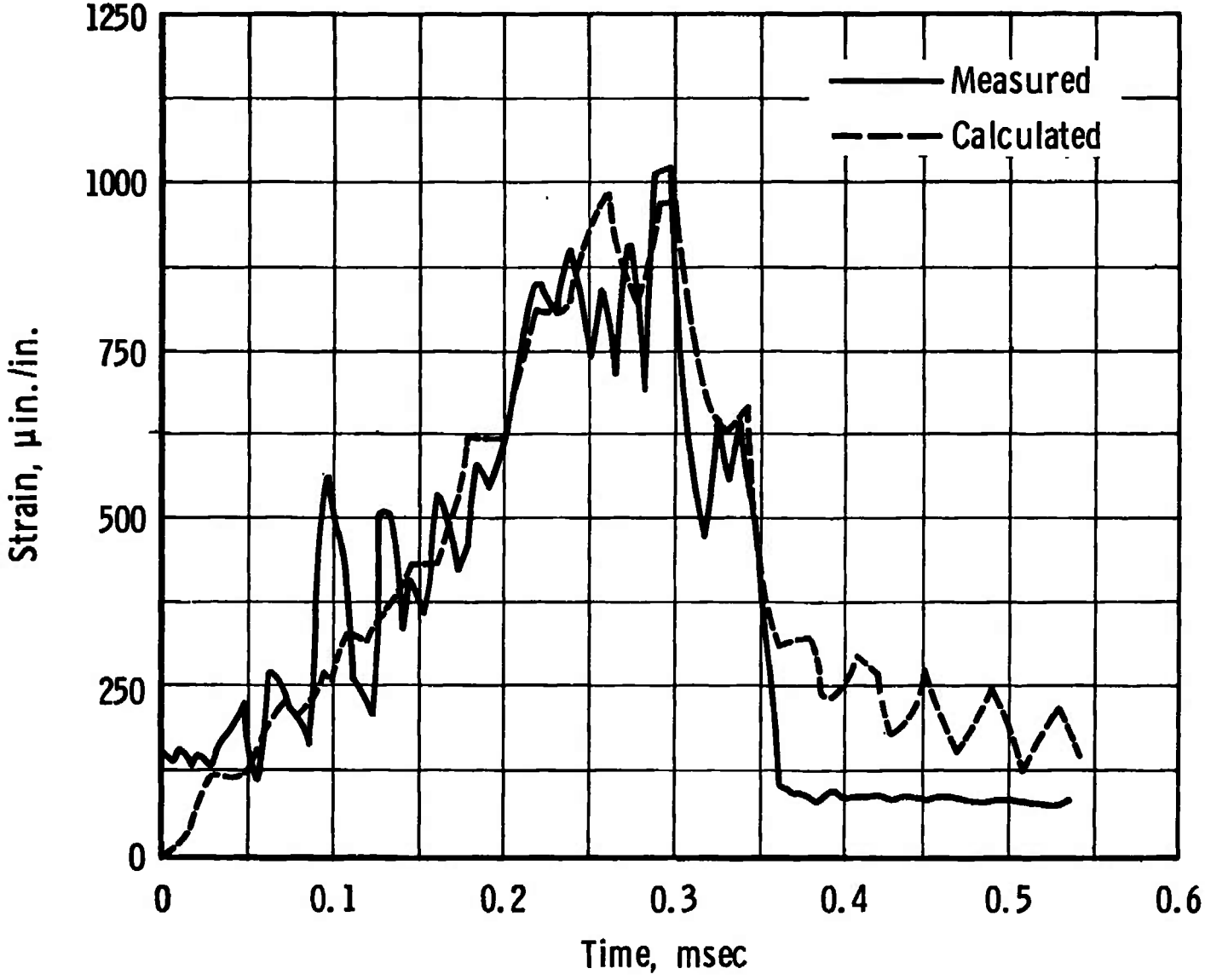

Fig. 8 Comparison of Measured and Calculated Strain for Shot T-1247

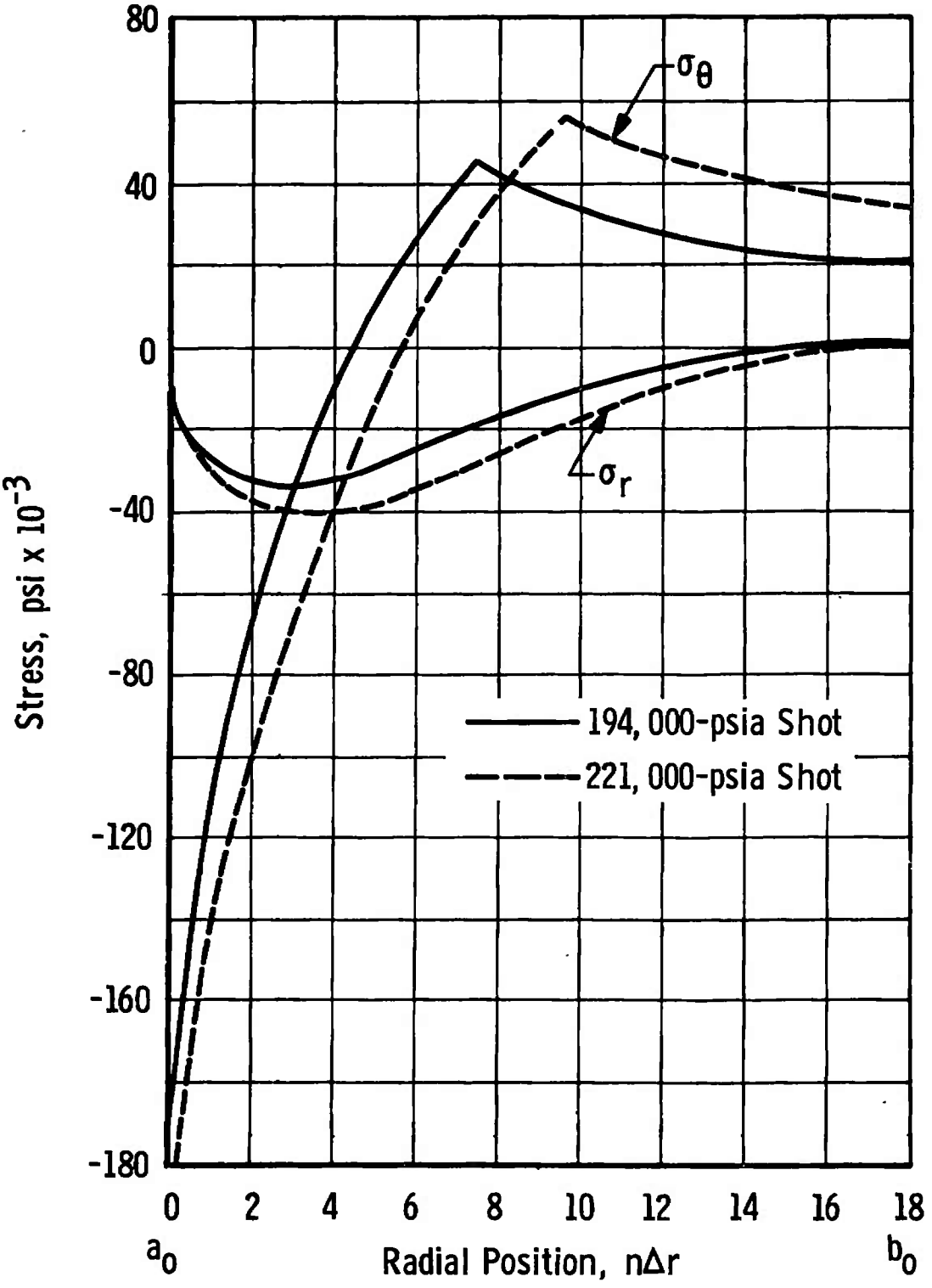

Fig. 9 Predicted Radial Distribution of Tangential and Radial Residual Stress after Lower Pressure Shot (194,000 psi) and Higher Pressure Shot (221,000 psi)

TABLE I
RADIAL GROWTH (DELR)

Shot Number	T-1247	T-1237
Non-Autofrettaged	5.5×10^{-3} in.	9×10^{-3} in.
Autofrettaged	0	0

TABLE II
PEAK TANGENTIAL STRAIN

Shot Number	T-1247	T-1237
Non-Autofrettaged	1600×10^{-6} in./in.	2098×10^{-6} in./in.
Autofrettaged	985×10^{-6} in./in.	1179×10^{-6} in./in.
Experimental	1030×10^{-6} in./in.	1020×10^{-6} in./in.

UNCLASSIFIED
Security Classification

DOCUMENT CONTROL DATA - R & D

(Security classification of title, body of abstract and indexing annotation must be entered when the overall report is classified)

1. ORIGINATING ACTIVITY *(Corporate author)*
Arnold Engineering Development Center
ARO, Inc., Operating Contractor
Arnold Air Force Station, Tennessee

2a. REPORT SECURITY CLASSIFICATION
UNCLASSIFIED

2b. GROUP
N/A

3 REPORT TITLE
PROPAGATION OF ELASTO-PLASTIC STRESS WAVES IN CYLINDRICAL HIGH-PRESSURE SECTIONS

4. DESCRIPTIVE NOTES *(Type of report and inclusive dates)*
Final Report - June 1968 to July 1969

5. AUTHOR(S) *(First name, middle initial, last name)*
J. R. Baumgarten, J. R. DeWitt, and A. J. Cable, ARO, Inc.

6. REPORT DATE	7a. TOTAL NO. OF PAGES	7b. NO. OF REFS
August 1970	33	9

8a. CONTRACT OR GRANT NO.	9a. ORIGINATOR'S REPORT NUMBER(S)
F40600-71-C-0002 b. PROJECT NO. 876 c. Program Element 65401F d. Task G226	AEDC-TR-70-42 9b. OTHER REPORT NO(S) *(Any other numbers that may be assigned this report)* ARO-VKF-TR-70-42

10. DISTRIBUTION STATEMENT
This document has been approved for public release and sale; its distribution is unlimited.

11. SUPPLEMENTARY NOTES	12. SPONSORING MILITARY ACTIVITY
Available in DDC	Arnold Engineering Development Center, Air Force Systems Command, Arnold Air Force Station, Tennessee

13. ABSTRACT This report presents an analysis of the axisymmetric elastic and plastic stresses and deformations in thick wall cylindrical shells subjected to internal dynamic pressures. A direct numerical approach called the discontinuous-step analysis is used. This analysis is based on the direct use of the boundary conditions and the applicable physical laws to propagate dynamic changes in the cylinder by finite steps. Reflection of stress waves from both inner and outer boundaries is automatically generated. The validity of the method is checked by comparison of numerical results in the elastic range with published results for thick wall cylinders. Comparison is made with experimentally measured strains from the high-pressure section of a hypervelocity launcher. This analysis assumes that the work hardening of the material is independent of the strain rate and is constant for a large variation of plastic strain. Stress-strain relationships are derived for the condition of plane stress in the cylinder which is held to be representative of the actual conditions in the launcher high-pressure section. The digital computer program developed from this study predicts the distribution of dynamic stress and strain throughout the cylinder, the internal radial growth, the distribution of particle displacement, the distribution of yield stress in an autofrettaged cylinder, and the residual stress.

DD FORM 1 NOV 65 1473

UNCLASSIFIED
Security Classification

14. KEY WORDS	LINK A		LINK B		LINK C	
	ROLE	WT	ROLE	WT	ROLE	WT
stress analysis						
elastic theory						
plastic theory						
high-pressure tests						
cylindrical shells						
hypervelocity guns						
numerical analysis						
dynamic structural analysis						

AEDC
Arnold AFS Tenn